PAPER • OPEN ACCESS

Modelling of shear bands during solidification

View the article online for updates and enhancements.

Modelling of shear bands during solidification

A Ludwig[1], C M G Rodrigues[1], M Wu[1] and A Kharicha[1,2]

[1] Chair of Simulation and Modelling Metallurgical Processes, Metallurgy Department, Montanuniversitaet Leoben, Franz-Josef Street 18, 8700 Leoben, Austria
[2] Christian-Doppler Laboratory for Metallurgical Application of Magnetohydrodynamics, Montanuniversitaet of Leoben, Franz-Josef Street 18, 8700 Leoben, Austria

E-mail: christian.gomes-rodrigues@unileoben.ac.at

Abstract. Major developments have been accomplished in the understanding of the physics involved in granular media and suspensions when subjected to shearing stresses. However, although partially solidified alloys have been reported to exhibit similar characteristics as granular material under certain conditions, such findings have never been fully addressed by the solidification community. Here, the modelling approaches adopted in granular mechanics for the description shear-induced particle migration have been included into a solidification model. It is shown that shear-induced particle migration has a considerable effect on the solid fraction distribution and macrosegregation formation in casting processes where a continuous and significant shear rate exists in a conduit with relatively small geometrical aspect ratio.

1. Introduction

Shear bands, the localization of deformation in certain regions of intense shearing, is a phenomenon that is commonly observed in compacted granular materials. There has been extensive research on the comprehension of the principles involved in such phenomenon through extensive experimental and theoretical studies. A good example of such mechanism is the so-called migration phenomenon. For relatively large particles, measurements taken in different geometrical configurations (e.g., in concentric Couette cells, parallel channels, etc.) have shown that the particles migrate irreversibly from high shear regions towards low shear regions [1-3]. It takes place in suspensions under steady uniform plane shear flows and has been successfully modelled both as a single fluid representing the whole suspension [4, 5] and as a two-phase model where the fluid and the particles are considered as two distinct interpenetrating continua [6, 7]. Although in both case good agreement with experimental data is obtained, the latter approach provides a more detailed description of the multiphase flow dynamics than the mixture models. This is an essential feature when complex phenomena are under scrutiny.

In solidification processes, besides the convection of the equiaxed crystals, a phase transition occurs to the melt which gradually transforms into solid. The rheology of the solid-liquid mixture changes considerably during this process. At low solid fractions, the behaviour of the solid-liquid mixture is described as suspensions and the flow is mainly dictated by the transporting character of the liquid phase. Within this regime, it is commonly accepted that the viscosity of the mixture varies exponentially with solid fraction [4, 8]. At a critical solid fraction, the crystals start to create bridges between one another, and the material develops into a coherent structure which has cohesive properties. This is where strength development of the material slowly begins [9]. With further solidification, the crystals become fully connected and the mush exhibits a more solid-like behaviour, which is often described as a viscoplastic continuous solid skeleton saturated with interstitial liquid [10]. In the latter regime (referred as

viscoplastic regime), particular constitutive equations are employed for the deformation of the mush that arises due to shrinkage, convection or imposed external loads. Due to its interest for casting production, both experimental and computational studies have been undertaken to analyse the deformation behaviour of semi-solids at high temperatures [11-13].

Interestingly, experimental research has shown that, under certain conditions, the rheology of equiaxed solidifying alloys exhibits similar characteristics as compacted granular materials at solid fractions below the viscoplastic limit [14]. Such results are particularly important because they explain the formation of casting defects, such as macrosegregation and porosity, in a solid fraction range that can have a major impact on the final solidified microstructure. To our knowledge, such findings have never been applied to models designed to replicate solidification processes.

In the present paper, the modelling approaches adopted in granular mechanics for the description of the rheological behavior of suspensions at moderate solid fractions under steady uniform plane shear flows have been integrated into a thermo-mechanical and macrosegregation solidification model to explore the principles behind shear-induced particle migration during solidification.

2. Model description

The solidification model has been described in detail in previous works [12, 15]. It includes also constitutive equations that replicate the deformation of the mush due to shrinkage, convection or imposed external loads. Under such conditions, the mush can either densify (by expelling liquid from its core) or dilate (by draining liquid from its surroundings), giving rise to local relative motion between the phases, and eventually leading to macrosegregation deviations in the cast products [12, 16, 17]. In the present paper, special attention is drawn to the formulation adopted to account for the shear-induced migration (SIM).

The origin of particle migrations is related to the pressure gradients experienced by the particles. In pressure-driven flows through a channel with homogeneous suspensions, shear rate is usually maximal near the walls, and decreases towards the centreline. This correlates with the higher granular pressure gradient near the walls, where particle-particle collisions are more frequent. As a result, a net body force arises on the solid phase that leads to an inward flux of particles which is compensated by an outwards flux of liquid. This persists until the granular pressure becomes homogenous across the section.

The migration mechanism is taken into account in the present model by mean of a shear-induced stress tensor, Σ_s, in the solid phase, which can be written as follows:

$$\Sigma_s = -\mu_l \eta^n \left(g_s \right) \dot{\gamma}_{eff} \mathbf{Q} \tag{1}$$

where μ_l is the liquid viscosity, $\dot{\gamma}_{eff} = \sqrt{2\dot{\boldsymbol{\varepsilon}} : \dot{\boldsymbol{\varepsilon}}}$ is the effective shear rate of the suspensions, and $\mathbf{Q}$ represents the anisotropy tensor [18] which in this work has been assumed as being equal to the identity tensor for simplicity. For the dimensionless particle viscosity, $\eta^n(g_s)$, the following expression is employed:

$$\eta^n \left(g_s \right) = K_n \left(\frac{g_s}{g_s^p} \right)^2 \left(1 - \frac{g_s}{g_s^p} \right)^{-2} \tag{2}$$

with $K_n = 1$ [19] and the packing solid fraction $g_s^p = 0.68$ [18].

Note that different closure models and parameters are often used for different configurations so that a better fit is achieved with measurements. However, not only this affects the generalizability of the results, it is also important to keep in mind that experimental data are not always possible, particularly in solidification processes. Therefore, in the present work, the same closure models and parameters are kept in all test cases performed so that an objective assessment of the model is carried out. Nevertheless, it is worth noting that, from the set of simulations performed for this paper, it has been found that manipulating the fitting parameters or using the anisotropic tensor, $\mathbf{Q}$, did not produce noteworthy changes in the results.

Contrary to the liquid phase, where the deviatoric stress tensor is given solely by its classical representation for incompressible Newtonian fluids (i.e., $\mathbf{\Sigma}_l^{eff} = \boldsymbol{\tau}_l = 2\mu_l \mathrm{dev}(\dot{\boldsymbol{\varepsilon}}_l)$), in the solid phase, the shear-induced stress tensor contribution is added to the deviatoric stress tensor, yielding:

$$\mathbf{\Sigma}_s^{eff} = \boldsymbol{\tau}_s = 2\mu_s \mathrm{dev}(\dot{\boldsymbol{\varepsilon}}_s) + \Sigma_s \tag{3}$$

where the shear rate is given by $\dot{\boldsymbol{\varepsilon}}_i = \tfrac{1}{2}\left(\nabla\mathbf{v}_i + \left(\nabla\mathbf{v}_i\right)^T\right)$ and the solid viscosity, μ_s, can be calculated from the power-law viscosity model of Ishii [8] as follows:

$$\mu_s = \mu_\ell / g_s \left(\left(1 - g_s/g_s^p\right)^{-2.5 g_s^P} - (1 - g_s) \right) \tag{4}$$

which assumes the validity of the mixture rule for a suspension as:

$$\mu_{sus} = g_s \mu_s + g_\ell \mu_\ell \tag{5}$$

Introducing equations (1), (2) and (4) into equation (3) gives the deviatoric stress tensor for the solid phase, which is then employed in the momentum conservation equation. Besides momentum, volume-average conservation equations of mass, species, and enthalpy are also solved for both liquid and solid phases. The equations are presented in table 1, where g denotes the volume fraction, ρ the density, $\mathbf{v}$ the velocity vector, p the shared pressure, Σ_i^{eff} the effective deviatoric stress tensor, $\mathbf{g}$ the gravity vector, c the species concentration, h the enthalpy per unit mass, $\mathbf{q}$ the heat flow vector, n the grain number density, and the subscripts i refer to either liquid (l) or solid (s). In each computational cell, the sum of solid and liquid volume fractions (g_s and g_l, respectively) is equal to one. Details on the different interphase exchange terms are given in references [12,15].

Table 1. Volume-Averaged Conservation Equations.

Mass conservation:	$\dfrac{\partial g_i \rho_i}{\partial t} + \nabla \cdot (g_i \rho_i \mathbf{v}_i) = \mp M_{\ell s}$	(6)
Momentum conservation:	$\dfrac{\partial g_i \rho_i \mathbf{v}_i}{\partial t} + \nabla \cdot (g_i \rho_i \mathbf{v}_i \mathbf{v}_i) = -g_i \nabla p + \nabla \cdot g_i \mathbf{\Sigma}_i^{eff} + g_i \rho_i \mathbf{g} \mp \mathbf{U}_{ls}^D \mp \mathbf{U}_{ls}^M$	(7)
Species conservation:	$\dfrac{\partial g_i \rho_i c_i}{\partial t} + \nabla \cdot (g_i \rho_i \mathbf{v}_i c_i) = \nabla \cdot (g_i \rho_i D_i \nabla c_i) \mp C_{\ell s}$	(8)
Enthalpy conservation:	$\dfrac{\partial g_i \rho_i h_i}{\partial t} + \nabla \cdot (g_i \rho_i \mathbf{v}_i h_i) = -\nabla \cdot \mathbf{q}_i \mp H_{\ell s}$	(9)
Grain transport:	$\dfrac{\partial n}{\partial t} + \nabla \cdot (\mathbf{v}_s n) = N_{\ell s}$	(10)

The two-phase Eulerian-Eulerian volume-average model employed in this work is based on the two-PhaseEulerFoam solver from OpenFOAM toolbox [20]. However, the original code has been greatly altered mainly to incorporate the viscoplastic regime (described in detail in reference [12]) and the shear-induced migration phenomenon, which were not supported by the solver. This includes (among other developments) the addition of the bulk viscosity in the viscous stress term, the adaptation of the Navier-Stokes equation to cope with the different rheological material behaviors depending on the regime, the calculation of the effective solid viscosity (equation 5) and the shear-induced stress tensor (equation 1).

The present work is focused on the analysis of the shear-induced migration phenomena and the conditions employed in the different test cases analyzed are such that the viscoplastic regime is most of the time not activated (the onset of the viscoplastic regime occurs at solid fractions above 0.57). In order to

simplify the analysis of the results and focus our attention solely on the shear-induced migration phenomena, the viscoplastic regime has been neglected from the simulations presented here.

3. Results and discussion

Numerical simulations are performed for both a pressure-driven flow of a suspension in a conduit of rectangular cross-section and a suspension flow in a cylindrical Couette cell, for which experimental validation results are available in the literature. The two setups are illustrated in figure 1.
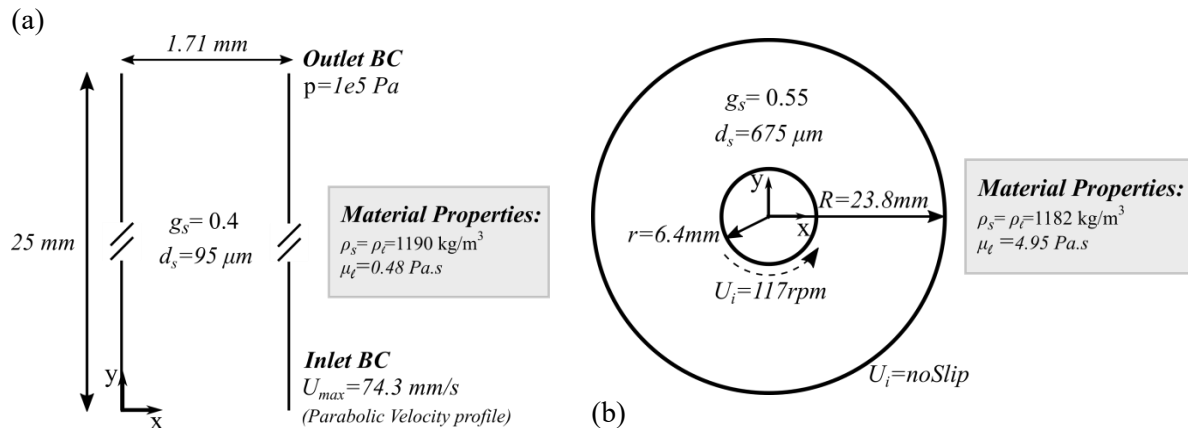
Figure 1. Schematic representation of (a) pressure-driven flow of a suspension in a conduit of rectangular cross-section, and (b) suspension flow in a cylindrical Couette cell.

In both cases, the simulations are performed in a 2D domain and gravity is neglected. Boundary conditions and material properties are defined in figure 1. A two-dimensional orthogonal mesh with 20×100 cells is used in the first case, whereas in the second, the mesh consists of 20 cells in the radial direction and 80 cells in the azimuthal direction (for one complete revolution).

3.1. Validation of results

The numerical results presented in this section are compared against well-known experimental measurements where particle migration has been observed.

Lyon and Leal [2] used a laser-Doppler velocimetry method (LDV) to measure both particle velocity and concentration profiles in a two-dimensional channel flow. The comparison between experimental data and the numerical results are presented in figure 2(a). It can be seen that an inhomogeneous particle distribution is obtained with high solid fraction being obtained along the centerline. The agreement between numerical and experimental results is in line with other comparisons reported in the literature (see e.g. [5] and [7]). Note that Lyon and Leal [2] reported that the particle concentration near the wall was lower than the true value because of the reduced signal-to-noise ratio in this region. This could justify the high discrepancy between numerical and experimental results in this region.

Phillips *et al.* [3] carried out nuclear magnetic resonance (NMR) imaging measurements of particle distributions for a monomodal suspension of polymethyl methacrylate spheres in a Newtonian solvent. Irreversible particle migration in the radial directions was observed. The comparison between experimental data and the numerical results after 200 revolutions of internal cylinder and initial solid fraction of 0.55 are presented in figure 2(b).
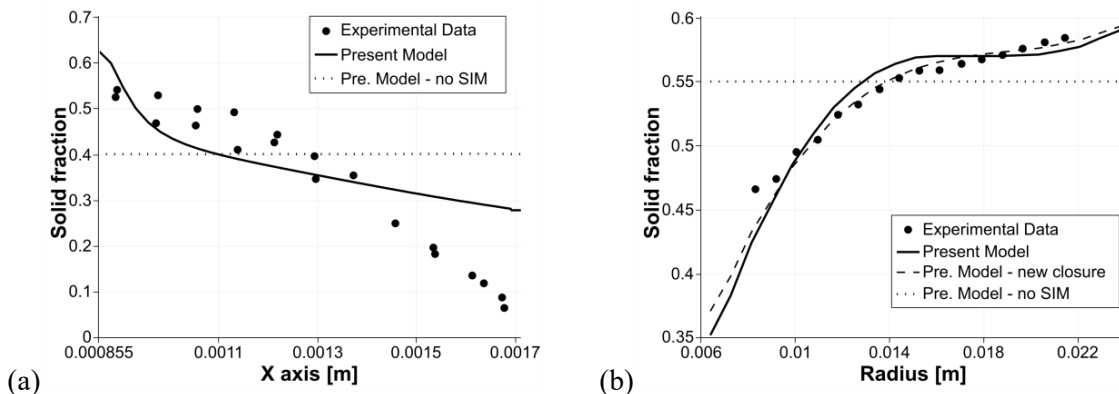
Figure 2. Simulation results for (a) 2D pressure-driven channel flow at y=0.192 for initial solid fraction of 0.4, compared against experimental data of Lyon and Leal [2], and (b) suspension flow in Couette cell after 200 revolutions of internal cylinder and initial solid fraction of 0.55, compared against experimental data of Phillips *et al*. [3]. Results with no shear-induced migration ("Pre. Model - no SIM") are also presented for reference.

The simulation displays a reasonable agreement with experimental data, although an overestimation of the measured solid fraction is observed in the middle of the domain. A better fit can, however, be obtained by assuming that $\mu_{sus} = \mu_s + \mu_l$ [18] – instead of the common mixture law applied in equation (4) – as presented in the dashed line (referred in the legend as "Pre. Model – new closure") of figure 2(b). These results raise some questions regarding the applicability the general rule of mixture for the viscosity employed in many research fields and in a wide range of the phase fraction, Reynolds number and flow regimes [21, 22]. Nevertheless, for the sake of consistency, the original approach is employed in the remainder of the paper.

A closer look at the above results reveals that the jamming effect in the parallel channel flow along the centerline is more significant than in the cylindrical Couette cell. Not only the shear rate is larger in the former configuration, it also keeps a constant value during the simulation since the velocity profile is imposed at the inlet. On the other hand, in the Couette cell, the suspension starts from a rest state which is then affected by the moving inner cylinder. However, as the velocity profile spreads towards the outer cylinder, the velocity gradient fades away, reducing with it the migration flux.

3.2. Effect of shear-induced migration during solidification processes
After having validated the shear-induced migration formulation, the main goal becomes understanding the potential effects of such phenomenon on solidification processes. The investigation of the transport and solidification phenomena occurring during the casting process is essential to avoid internal defects and improve the quality of casting strips. The relative motion between the phases – which might occur during SIM – can be an important source for such defects.

Solidification processes where SIM might be relevant should involve significant and continuous shear rates to the solidifying mush within a narrow and relatively long conduit. High-pressure die casting [14] and thixocasting process are potential examples where such conditions may apply. In the following, a cooling rate is applied on the walls of two parallel plates, in a configuration similar to the one presented in figure 1(a). Such conditions are pertinent in segments of both processes mentioned above, although lower velocity and pressure are assumed here for simplicity. This analysis should provide some insight on how SIM can affect the results, even under simplified conditions. A schematic representation of the domain is illustrated in figure 3 and the simulations are performed for the Al-7wt% Si alloy.
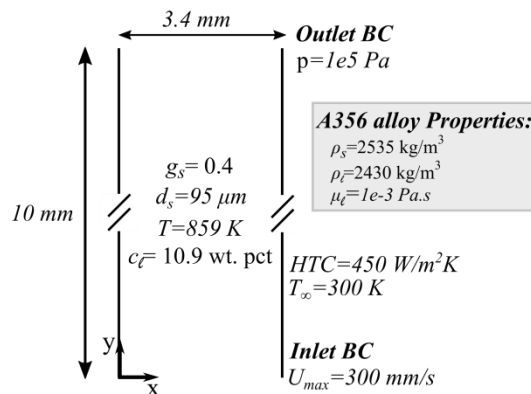
Figure 3. Schematic representation of test case involving shear-induced
migration and solidification of A356 alloy.

Figure 4 illustrates the solid fraction profile along a horizontal line located near the outlet. It can be seen that the simulation that considers solidification but neglects SIM ("Pre. model - no SIM") has increased solid fraction values near the walls, while the center maintains a lower value. Such distribution contrasts with the simulation that does not consider solidification of the melt but takes into account SIM ("Pre. model - no Sol"), which presents a solid fraction distribution similar to the pressure-driven channel flow presented above (in figure 2(a)). This means that a jamming of solid particles occurs along the centerline, whereas the solid fraction decreases near the walls. Also, the results of a simulation with no SIM and no solidification are presented in figure 4 for reference ("Pre. model – no SIM + no Sol").

In comparison with the case with no SIM, it can be seen that the solid fraction profile of the complete simulation ("Present model") changes dramatically. The solid fraction distribution maintains some characteristics of the SIM mechanisms, while increasing the general amount of particles along the cross section due to solidification. Due to the larger solidification rate near the walls, the difference in solid fraction between these results is also larger in that region than in the center.
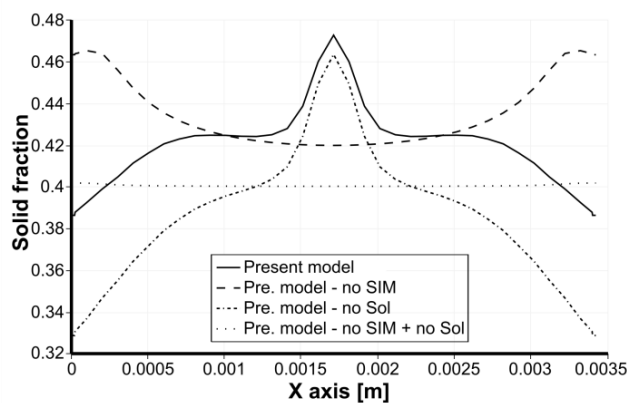
Figure 4. Steady state results of solid fraction distribution along
horizontal line located near outlet.

SIM mechanism induces a flux of particles towards the center, with an opposite flux of melt going towards the walls. Solidification growth, in turn, requires an inflow of material predominantly towards the walls to feed solidification. These two mechanisms create a relative motion between the two phases that influence macrosegregation, as observed in figure 5.
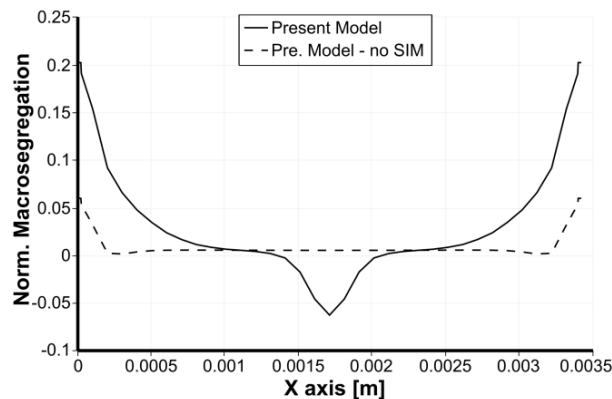
Figure 5. Steady state results of normalized macrosegregation along horizontal line located near the outlet.

Figure 5 illustrate the normalized macrosegregation distribution along the cross section of the conduit (near the outlet). The present results are also compared against the simulation that neglects SIM. In the latter case, a typical macrosegregation profile is observed. A positive composition deviation occurs near the walls, which is due to inverse segregation.

On the other hand, the present results show an increased positive deviation near the walls, while a negative deviation occurs along the centreline. Although inverse segregation plays a role near the wall, the positive deviation is mostly due to the migration effect taking place in this region, which replaces solid particles with solute-enriched melt. In turn, the negative macrosegregation formation along the centreline is the corresponding opposite effect, as the higher solid fraction region is associated with an inflow of crystals and an outflow of melt. The mechanism leading to this macrosegregation formation is similar to the one observed in ingot castings, where negative composition deviations are typically observed at the bottom due to the sedimentation of equiaxed crystals [15].

4. Conclusion

Sophisticated modelling approaches have been successfully employed in the field of granular media to simulate shear bands and, particularly, shear-induced migration. However, despite the fact that partially solidified alloys have been reported to exhibit similar characteristics as granular material, such deformation of the mush has never been addressed in solidification process. Here, the constitutive laws employed for predicting shear-induced migration have been included into a solidification model. The results show that particle migration is actually significant in the configurations where a continuous shear rate is imposed to the solidifying mush within a narrow and relatively long conduit.

References
[1]   Leighton D and Acrivos A 1986 *Chem. Eng. Sci.* **41** 1377–84
[2]   Lyon M K and Leal L G 1998 *J. Fluid Mech.* **363** 57–77
[3]   Phillips R J, Armstrong R C, Brown R A, Graham A L and Abbott J R 1992 *Phys. Fluids A.* **4** 30–40
[4]   Nott P R, Guazzelli E and Pouliquen O 2011 *Phys. Fluids* **23** 043304-13
[5]   Dbouk T, Lemaire E, Lobry L and Moukalled F 2013 *Fluid Mech.* **198** 78–95
[6]   Drijer I, van de Laar T, Vollebregt H M and Schroën C G P H 2018 *Sep. Purif. Technol* **192** 99–109

[7]   Municchi F, Nagrani P P and Christov I C, 2019 *Int. J. Multiph. Flow* **120** 103079-15
[8]   Ishii M 1977 ANL-77–47
[9]   Dahle A K and StJohn D H 1998 *Acta Mater.* **47** 31–41
[10]   Martin C L, Favier D and Suéry M 1999 *Int. J. Plast*. **15** 981–1008
[11]   Nguyen T G, Favier D and Suery M 1994 *Int. J. Plast*. **10** 663–93
[12]   Rodrigues C M G, Ludwig A, Wu M, Kharicha A and Vakhrushev A 2019 *Metall. Mater. Trans. B* **50** 1334–50
[13]   Rodrigues C M G, Ludwig A, Wu M, Kharicha A and Vakhrushev A 2019 *Preprint*
[14]   Gourlay C M and Dahle A K 2007 *Nature* **445** 70–73
[15]   Ludwig A and Wu M 2002 *Metall. Mater. Trans. A* **33** 3673–83
[16]   Fachinotti V D, Le Corre S, Triolet N, Bobadilla M and Bellet M 2006 *Int. J. Numer. Meth. Eng.* **67** 1341–84
[17]   Rodrigues C M G R, Ludwig A, Kharicha A, Wu M and Vakhrushev A 2019 *IOP Conf. Mater. Sci. Eng.* **529** 1-7
[18]   Morris J F and Boulay F 1999 *J. Rheol*. **43** 1213–37
[19]   Boyer F, Guazzelli É and Pouliquen O 2011 *Phys. Rev. Lett*. **107** 1–5
[20]   Greenshields C J, 2018 OpenFOAM – The OpenFOAM Foundation – User Guide, http://foam.sourceforge.net/docs/Guides-a4/OpenFOAMUserGuide-A4.pdf
[21]   Beckermann C and Viskanta R 1993 *Appl. Mech. Rev*. **46** 1–27
[22]   Wu M, Ludwig A and Kharicha A 2019 *Metals* **9** 229 1-43